A novel approach to sulfate geoengineering with surface emissions of carbonyl sulfide

Ilaria Quaglia[1], Daniele Visioni[2], Giovanni Pitari[1], and Ben Kravitz[3,4]

[1]Department of Physical and Chemical Sciences, Universitá dell'Aquila, 67100 L'Aquila, Italy
[2]Sibley School for Mechanical and Aerospace Engineering, Cornell University, Ithaca, NY 14853, USA
[3]Department of Earth and Atmospheric Science, Indiana University, Bloomington, IN, USA
[4]Atmospheric Sciences and Global Change Division, Pacific Northwest National Laboratory, Richland, WA, USA

Correspondence: Ilaria Quaglia (ilaria.quaglia@aquila.infn.it)

Abstract. Sulfate geoengineering (SG) methods based on lower stratospheric tropical injection of sulfur dioxide (SO_2) have been widely discussed in recent years, focusing on the direct and indirect effects they would have on the climate system. Here a potential alternative method is discussed, where sulfur emissions are located at the surface in the form of carbonyl sulfide (COS) gas. A time-dependent chemistry-climate model experiment is designed from year 2021 to 2055, assuming a 40 Tg-S/yr artificial global flux of COS, geographically distributed following the present day anthropogenic COS surface emissions. The budget of COS and sulfur species is discussed, as well as the effects of SG-COS on the stratospheric sulfate aerosol optical depth ($\Delta\tau$=0.080 in years 2046-2055), aerosol effective radius (0.46 μm), surface SO_x deposition (+8.7 %) and tropopause radiative forcing (RF) (-2.0 W/m^2 for clear sky conditions and -1.5 W/m^2 including the cloud adjustment). Indirect effects on ozone, methane and stratospheric water vapor are also considered, along with the COS direct contribution (with an overall gas phase global radiative forcing of +0.23 W/m^2). According to our model results, the resulting net RF of this SG-COS experiment is -1.3 W/m^2 for the year 2050, and it is comparable to the corresponding RF of -1.7 W/m^2 obtained with a sustained injection of 4 Tg-S/yr in the tropical lower stratosphere in the form of SO_2 (SG-SO2, able to produce a comparable increase of the sulfate aerosol optical depth). Significant changes of the stratospheric ozone response are found in SG-COS with respect to SG-SO2 (+4.9 DU versus +1.5 DU, globally). According to the model results, the resulting UVB perturbation at the surface accounts to -4.3% as a global-annual average (versus –2.4% in the SG-SO2 case), with a springtime Antarctic decrease of -2.7% (versus a +5.8% increase in the SG-SO2 experiment). Overall, we find that an increase in COS surface emission may be feasible, and produce a more latitudinally-uniform forcing without the need for the deployment of stratospheric aircrafts.

1 Introduction

Reducing part of the incoming solar radiation (known as Solar Radiation Modification, SRM) has been proposed as a short-term strategy for reducing surface temperatures and thus mitigating some of the worst side-effects of the greenhouse gases-induced global warming (Budyko, 1978; Crutzen, 2006). Various methods have been proposed to achieve this: the injection of sulfate precursors into the lower stratosphere to obtain an optically-active cloud of aerosols has been, by far, the most studied due to the observation of a similar cooling effect produced by explosive volcanic eruptions in the past (Robock, 2000). While preliminary

estimates for the cost of an eventual deployment already exist (Smith and Wagner, 2018), from an engineering perspective

25 there are no known technologies readily available to carry SO_2 or any other precursors considered up to now from the ground up to the lower stratosphere in the quantities needed to obtain a noticeable effect on the surface climate (Lockley et al., 2020). Since any proposed compound would quickly react to form sulfate aerosols, they would need to be carried sealed to the desired altitude, and then released, to ensure a high enough lifetime compared to that of the same aerosols in the troposphere (Lamarque et al., 2013).

30 We propose here a different approach to increasing the aerosol optical depth in the stratosphere, that makes use of bottom-up emissions of a gaseous precursor of sulfate aerosols: carbonyl sulfide (COS). COS has a long atmospheric lifetime (4 to 6 years; Khalil and Rasmussen, 1984; Ulshofer et al., 1996) due to its very low reactivity in the troposphere. Because of this, it is also uniformly mixed in the atmosphere, with an average concentration of 0.5 ppbv, and therefore it easily reaches the stratosphere: in quiescent volcanic conditions, COS is the main contributor of sulfate aerosols in the Junge layer (Bruhl et al., 2012), where

35 after photodissociation by ultraviolet light and oxidation processes, it is turned into SO_2 and subsequently oxidized into sulfuric acid, forming sulfate aerosols (Crutzen, 1976). It is naturally produced by various biological processes and environments, such as saline ecosystems, rainwaters (Mu et al., 2004) and biomass burning. Furthermore, it is also produced in various industrial processes (Lee and Brimblecombe, 2016) after CS_2 is oxidized. Its chemical life is very long (35 years; Bruhl et al., 2012) and thus its main sink is the uptake from oxic soils (Kuhn and Kesselmeier, 2000; Steinbacher et al., 2004) and vegetation

40 (Sandoval-Soto et al., 2005). In the concentrations found in the atmosphere, it is not a toxic gas for humans or ecosystems: negative effects have been found only when concentration exceed 50 ppm (100,000 times more than the background mixing ratio (Kilburn and Warshaw, 1995; Bartholomaeus and Haritos, 2006).

For these reasons, we investigate in this work the possible use of COS as a precursor to stratospheric sulfate aerosols aimed at reducing part of the incoming solar radiation. With the use of the University of L'Aquila-Climate-Chemistry Model

45 (ULAQ-CCM) we investigate the possible increase of COS surface fluxes to obtain a stratospheric aerosol optical depth (AOD) similar to that obtained with the injection of 8 Tg-SO_2 in the stratosphere. Together with assessing the resulting optically thick aerosol cloud, we also explore the eventual side-effects on key chemical components in the atmosphere, in order to determine how the side effects from COS-induced Sulfate Geoengineering (SG-COS) compare with those from SO_2-induced Sulfate Geoengineering (SG-SO2). For the latter, there is ample literature assessing its effect on stratospheric ozone (Tilmes et al.,

50 2008; Pitari et al., 2014; Xia et al., 2017a; Vattioni et al., 2019): the increase in surface area density, stratospheric heating and dynamical effect all play a part in determining the overall changes (Tilmes et al., 2018b; Richter et al., 2017) to the ozone column that, in turn, determine the changes in surface UV (Visioni et al., 2017b; Madronich et al., 2018) that would be important when considering adverse health effects (Eastham et al., 2018).

2 Model description and setup of numerical experiments

55 The simulations presented in this paper have been carried out with the University of L'Aquila Climate-Chemistry Model (ULAQ-CCM), a CCM robustly tested and used before in evaluation of the radiative, chemical and dynamical effects of

stratospheric and tropospheric aerosols (Pitari et al., 2002; Eyring et al., 2006; Morgenstern et al., 2010). It has also been used for various sulfate geoengineering simulations (Pitari et al., 2014; Visioni et al., 2018a, b) and, as part of the Climate-Chemistry Model Intercomparison project (Morgenstern et al., 2018), where it has been extensively validated with other CCMs.

60 The high vertical resolution (127 levels) allows for a proper representation of large-scale transport of gas and aerosol species in the troposphere (Orbe et al., 2018) and in the stratosphere (Visioni et al., 2017b; Eichinger et al., 2019), and the detailed chemistry, including heterogeneous chemical reactions on sulfuric acid aerosols, polar stratospheric cloud particles, upper tropospheric ice and liquid water cloud particles allows for a full assessment of the effects of the increased sulfate burden on the atmospheric composition. ULAQ-CCM simulated COS also compares reasonably well with available measurements of

65 seasonal COS concentrations (see Fig. S1) from Kuai et al. (2015), with an average annual error of 6.5%, albeit with peaks in some areas and months of up to 30%.

In addition to a reference historical model experiment (1960-2015), we performed three sets of simulations: a baseline unperturbed (BG) case and two geoengineering experiments (SG-COS and SG-SO2), all run between the years 2021-2055, with analyses focusing on the 2046-2055 decade; all experiments take place under the Representative Concentration Pathway

70 6.0 (RCP; Meinshausen et al., 2011) emissions.

The first geoengineering experiment, SG-COS, tries to produce a significant stratospheric aerosol burden by enhancing current surface emission sources of COS by up to 40 Tg-S/yr. These emissions are located at the ground, in the main regions of anthropogenic COS surface emissions (see Fig. 1). The second experiment, SG-SO2, is very similar to previous experiments discussed in the literature, primarily by Kravitz et al. (2011) in the G4 experiment, and consist of the injection of a fixed yearly

75 amount of SO_2 (4 Tg-S/yr) at the equator, between 18 and 25 km of altitude.

For the geoengineering experiments, ULAQ-CCM is driven by time-dependent sea surface temperatures (SSTs) from the Community Climate System Model – Community Atmosphere Model version 4 (CCSM-CAM4; Neale et al., 2013), an atmosphere-ocean coupled model that ran similar geoengineering experiments as in SG-SO2 (described by Tilmes et al., 2015): this allows for the inclusion of the cooling produced by geoengineering on the surface to the assessment of the dynami-

80 cal and chemical effect as simulated by ULAQ-CCM. To include the important radiative effects produced by other atmospheric components (mainly, geoengineering-driven changes in greenhouse gases concentration and in ice clouds ; Visioni et al., 2017b, 2018a) the radiative module of ULAQ-CCM calculates at each time-step the surface temperature perturbation produced by the radiative flux changes induced by these components and includes them in the CCSM-CAM4 SSTs. This approach has been further explained and validated by Visioni et al. (2018a). While the prescribed SST setup has been shown to correctly

85 capture dynamical changes produced by SRM (Visioni et al., 2017b), it clearly does not capture potential feedbacks that may be relevant for surface climate, such as those produced by the different latitudinal distribution of the aerosol optical depth that we will show later on. These differences may also in turn feed back onto changes in COS lifetime through precipitation changes (Whelan et al., 2016) which we can't consider here. We will therefore limit ourselves to analyzing changes in atmospheric composition and dynamics, and how those contribute to the overall radiative forcing from the aerosols. Future experiments

90 with a more comprehensive Earth-system model will be necessary to determine the full extent of the climatic response.
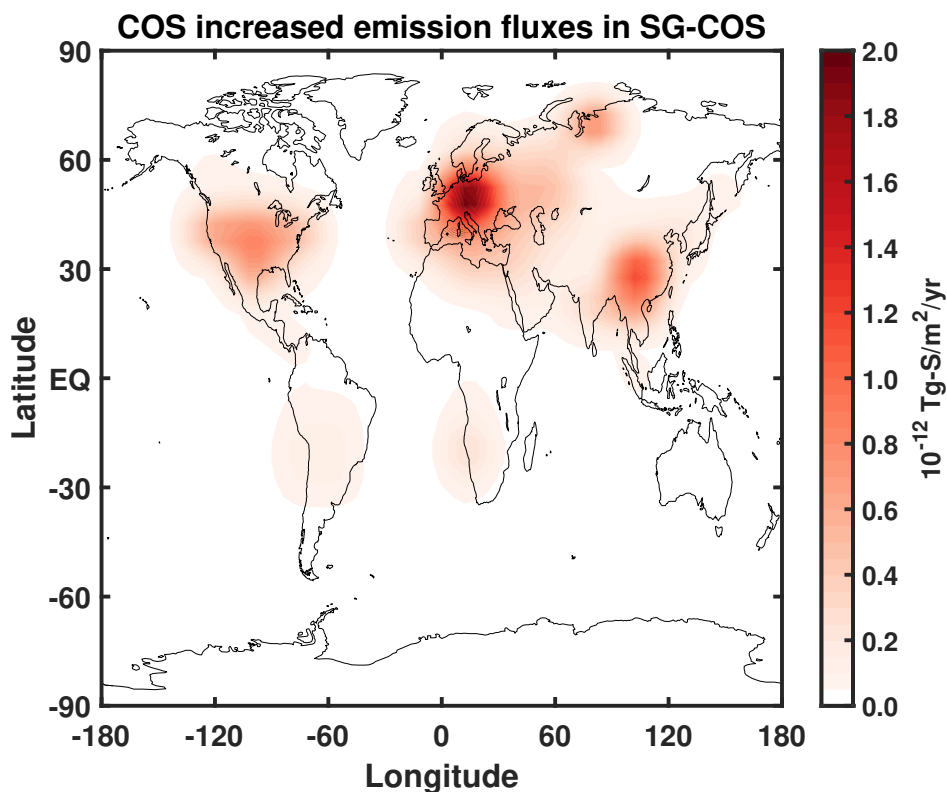
Figure 1. Geographical distribution of COS emission fluxes per year and unit of surface area (10^{-12} Tg-S/m^2/yr) in the SG-COS experiment. The annual upward flux is averaged over the period 2046-2055.

3 Results

3.1 Sulfate burden

COS is the most abundant sulfur-containing species in the atmosphere under quiescent conditions (i.e. not considering explosive volcanic eruptions). It is efficiently lost at the surface via dry deposition on soils and vegetation: taking this sink into account,

95 the net global lifetime (atmospheric chemistry plus surface deposition) is approximately 4 years, depending on the assumed magnitude of the soil and vegetation sink (Sandoval-Soto et al., 2005; Van Diest and Kesselmeier, 2008). In the troposphere the COS chemical reactivity (mostly with the hydroxyl radical) is rather slow: COS is thus well mixed and is easily transported in the stratosphere through the tropical tropopause layer (TTL). In the mid-stratosphere COS becomes efficiently photolyzed by solar UV radiation, becoming an important source for stratospheric SO$_2$ and finally for sulphuric acid aerosols.

100   When increasing the emission fluxes in SG-COS, it takes ~ 15 years before the concentration reaches a new equilibrium, from 0.5 to 35.5 ppbv (Fig. 2a). In the same timespan, the global AOD increases, reaching a value of 0.08 by 2035, similar to the global value that is reached by the direct injection of SO$_2$ in the equatorial stratosphere in SG-SO2; in that case, however,

the steady-state value is reached in only 1-2 years. At the end of 2055, the increased COS emissions and SO_2 injections are stopped. Average tropospheric COS concentrations follow an exponential decay guided by the tropospheric lifetime (3.8 years,

105   due to chemistry and soil deposition), reaching a value of 1.3 ppbv after 20 years (during 2075). This means an increase of 0.8 ppbv with respect to background condition, that would produce a direct RF negligible if compared to other well mixed greenhouse gases. The exponential decay of the stratospheric AOD in SG-COS is regulated by the stratospheric lifetime of COS (~10 years) mainly due to reaction with OH and photolysis, from which stratospheric SO_2 and finally sulphuric acid aerosols are formed. Therefore, the e-folding time for stratospheric AOD is longer with respect to the one resulting from

110   SG-SO2 (Fig. 2b). In 2075, the global stratospheric AOD reaches in SG-COS a value of 0.01, with respect to 0.003 in the background case.
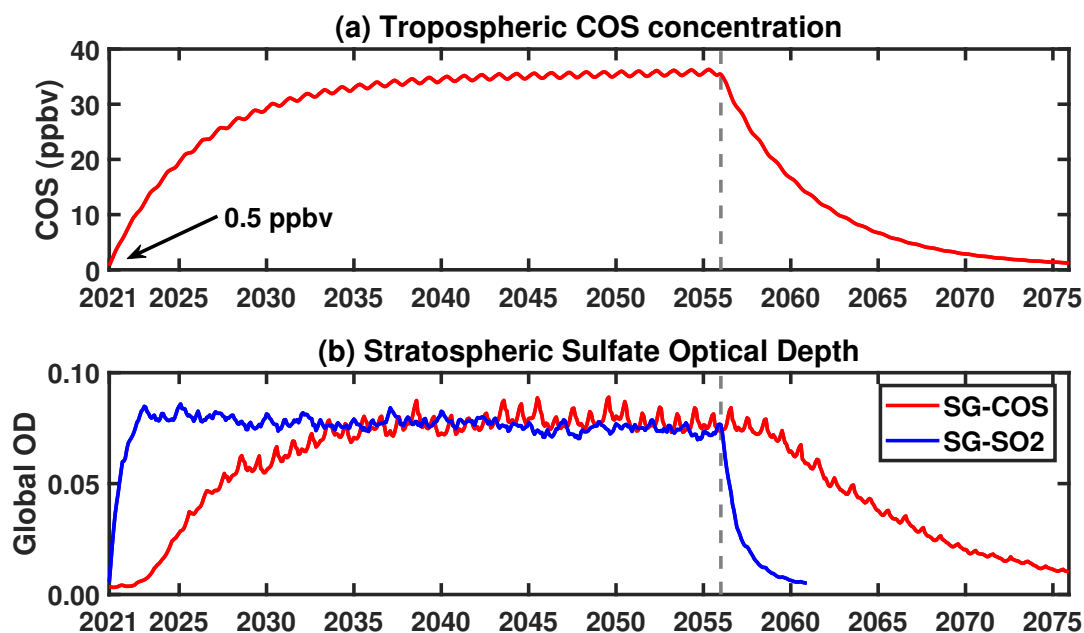
Figure 2. a) Monthly values of globally averaged tropospheric COS volume mixing ratio (ppbv) in SG-COS. The background value of 0.5 ppbv at the beginning of the simulation is highlighted. b) Globally averaged stratospheric sulfate optical depth monthly values in SG-COS (red) and SG-SO2 (blue). The grey line indicates the time when emissions of COS and SO_2 are stopped, at the end of 2055.

3.2 Sulfate aerosol properties

	BG	SG-COS	SG-SO2	SG-COS - BG	SG-SO2 - BG
Total Sulfate OD	0.055±0.003	0.135±0.004	0.130±0.003	0.080±0.004	0.075±0.004
Tropospheric Sulfate OD	0.052±0.003	0.057±0.003	0.055±0.003	0.005±0.004	0.003±0.004
Stratospheric Sulfate OD	0.003±0.001	0.078±0.002	0.075±0.001	0.075±0.002	0.072±0.001
Sulfate effective radius (μm)	0.18±0.01	0.46±0.01	0.63±0.01		
Ice OD	0.596±0.006	0.579±0.007	0.573±0.006	-0.017±0.009	-0.023±0.008
Ice effective radius (μm)	35±1	33±1	32±1		

Table 1. Summary of calculated sulfate aerosol and cirrus ice globally-annually averaged quantities relevant for RF calculations (i.e., optical depth at λ=0.55 μm and effective radius). Last two columns show the calculated SG changes with respect to the BG case [years 2046-2055].

In the SG-COS experiment, surface COS fluxes are adjusted so as to have the same global aerosol optical depth (AOD) ≈ 0.08 (see table 1). This is done in order to more easily compare the latitudinal distribution of the aerosols, and to better quantify
115 the differences in the radiative forcing from both direct and indirect (ozone, methane and water vapor) changes in atmospheric composition.

There is a large difference in the latitudinal distribution of stratospheric sulfate optical depth, as shown in figure 3 (a). SG-COS produces an AOD more uniformly distributed over all latitudes with respect to the SG-SO2 case, where the increase of optical depth is most prominent in the tropics; this is due to the efficient tropospheric mixing of COS before it reaches the
120 stratosphere.

The differences in the latitudinal distribution of AOD are also observable in the differences in the particle sizes and in the surface area density (SAD). Figure 3 (b) shows that the stratospheric effective radius is smaller in the SG-COS experiment and uniform for all latitudes, with a global value of 0.46 μm. In SG-SO2, the effective radius is higher in the tropics (0.63 μm); AOD is also larger in the tropics in that case, due to a larger concentration of particles there, even if larger particles are less
125 effective at scattering incoming solar radiation (English et al., 2012).

Figure 4 shows a comparison of the effective radius (a) and SAD (b) between the BG, SG-COS and SG-SO2 cases, separating the tropics, mid-latitudes and polar regions. As SO$_2$ is injected at the equator, all oxidation and nucleation happens in the tropics in SG-SO2. This is reflected in the vertical distribution which has a maximum in the lowermost stratosphere. On the other hand in SG-COS, the effective radius increase is reached at higher altitudes, between 18-30 km, which is consistent with COS
130 reaching higher altitudes through deep tropical convection before it is photochemically destroyed (Barkley et al., 2008). The same explanation is valid for the tropical SAD in panel (b).

As the size of the particles is determined by nucleation in the tropical region, where SO$_2$ oxidation occurs, mid-latitude and polar behaviour of the aerosols depends on the polewards transport by the Brewer-Dobson Circulation (BDC).

In SG-SO2, aerosols grow rapidly in the tropical region due to the high concentration of SO_2, and their larger size affects
135   sedimentation rates, thus decreasing their lifetime. Consequently, the amount of aerosols transported to higher latitudes is
lower; in SG-COS, smaller particles with a higher lifetime are either easily transported towards the poles or directly formed
there. Smaller particles at a higher concentration, and larger particles at a lower concentration may then result in a SAD which
looks similar at mid-latitudes and polar region, but for different reasons.

The vertical distribution of particles and their optical properties are shown in Figure 5 (see Fig. S2 for COS, SO_2 and
140   SO_4 concentration changes). The vertical distribution of the SAD is fundamental to understand the role of the heterogeneous
reaction and their effect on stratospheric ozone. The baseline case in panels (a) and (b) are a reference for understanding their
changes in SG-COS (panels (c) and (d)). The particles transported via the BDC to the poles are large enough to efficiently
scatter solar radiation so that the SAD and extinction changes show a similar behaviour, with a global increase of stratospheric
values with maxima at higher latitudes between 15-25 km.

145   Panels (f) and (d) show the extinction and SAD changes between the two SG experiments, to underline that in SG-SO2
extinction of the radiation is confined in the tropical stratosphere between 15-25 km, meaning a negative change in SG-COS.
As discussed before, the formation of larger particles in SG-SO2 in the tropical region reduces the amount of aerosol transported
to the poles compared to the SG-COS case, where a larger number of smaller particles produces a positive change in SAD and,
consequently, in extinction.

150   **3.3   Deposition**

Experiment	MSA	SO_2	SO_4	COS	CS_2	H2S	Total
BG	1.0±0.1	35.2±1.4	9.4±0.4	0.39±0.01	0.47±0.03	1.5±0.1	48.0±1.8
SG-SO2	1.0±0.1	35.6±1.5	9.5±0.4	0.39±0.01	0.47±0.03	1.5±0.1	48.5±1.8
SG-COS	1.0±0.1	36.4±1.5	9.9±0.4	31.6±0.1	0.47±0.03	1.5±0.1	80.9±1.7

Table 2. Globally-annually averaged dry deposition rates of sulfur species (Tg-S/yr) [years 2046-2055].
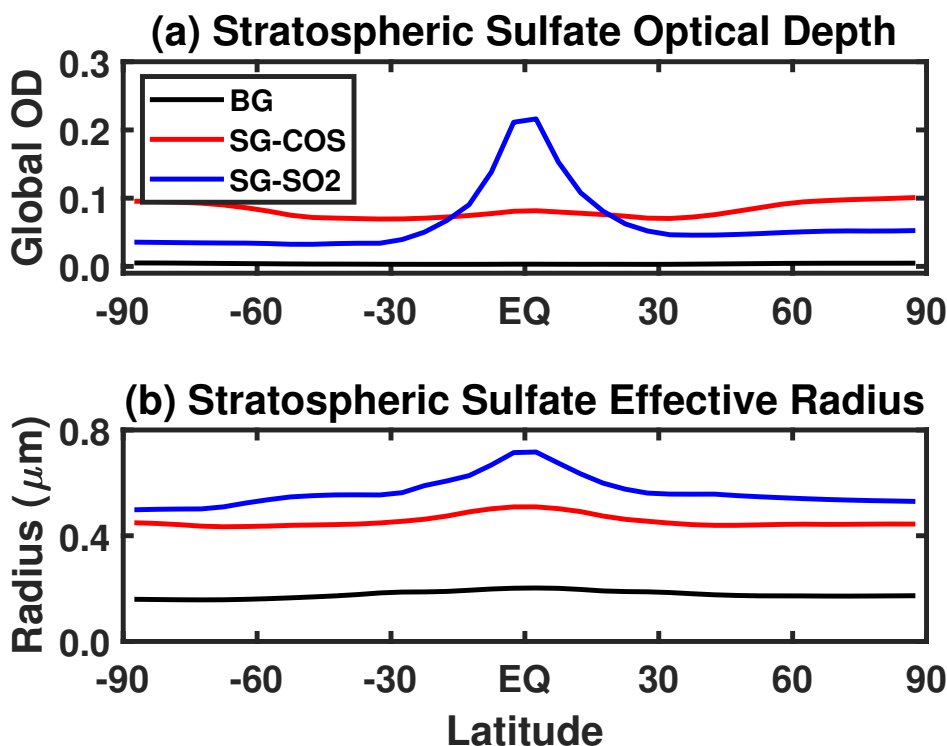
Figure 3. a) Latitudinal distribution of zonal mean values of stratospheric sulfate optical depth for the BG (black), SG-COS (red) and SG-SO2 (blue) cases. b) Stratospheric effective radius (in μm) (from tropopause to 6hPa). All quantities are annually averaged over the years 2046-2055.

Experiment	MSA	SO$_2$	SO$_4$	Total	Net [sources-sinks]
BG	1.5±0.1	3.0±0.1	43.2±1.5	47.7±1.6	+0.3±0.1
SG-SO2	1.5±0.1	3.2±0.1	46.5±1.5	51.2±1.6	+0.5±0.1
SG-COS	1.5±0.1	3.4±0.1	49.4±1.5	54.3±1.6	+0.8±0.1

Table 3. Globally-annually averaged wet deposition rates of sulfur species (Tg-S/yr) [years 2046-2055]. The last column shows the net balance of total sulfur sources and sinks (Tg-S/yr).

The enhancement of the stratospheric sulfate burden would produce an increase in sulfur deposition, in dry form through acid gas deposition and in wet form through rain, fog and aerosol particles.

Acid deposition may damage human health when high concentrations of particles with a diameter below certain thresholds (PM2.5 and PM10) are inhaled. The acidification of soils and water may damage plants, microorganisms and aquatic animals,

(a) Sulfate Effective Radius

(b) Sulfate SAD
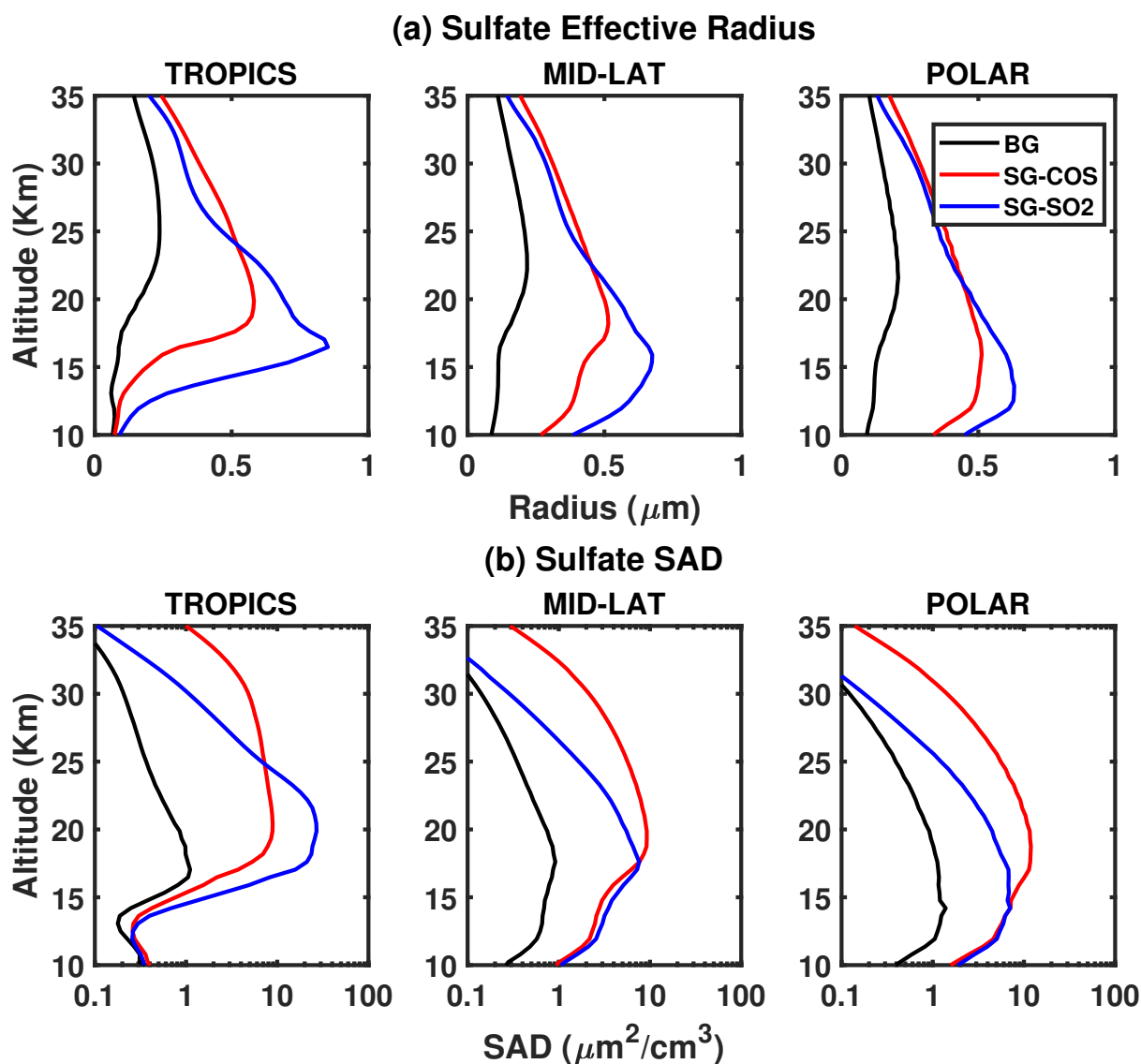
Figure 4. Vertical profiles of sulfate effective radius (in μm, a) and surface area density (in μm^2/cm^3, b) at different latitudinal bands (20N-20S for the Tropics, 30-50 at both N and S for the Mid-lat and 60-90 at both N and S for the Polar plots). All quantities are annually averaged over the years 2046-2055.
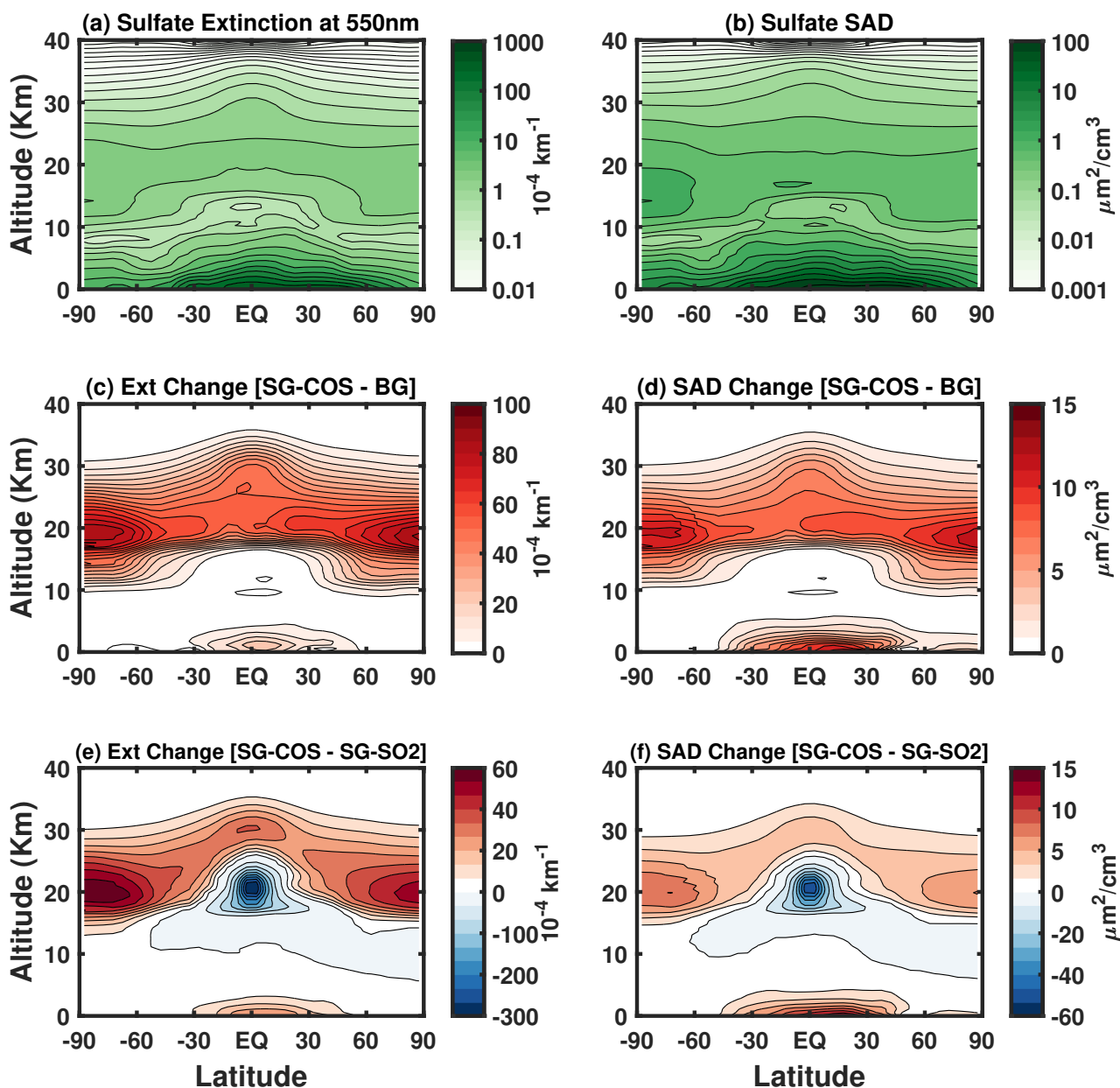
Figure 5. Zonal mean values of sulfate extinction (in 10^{-4} km^{-1}) and SAD (in μm^2/cm^3) in BG (panels a and b, respectively) and their change in the case of the SG-COS experiment (panels c and d). Panels e) and f) show extinction and SAD changes between SG-COS and SG-SO2. All quantities are annually averaged over the years 2046-2055.

155   but the impact on the ecosystem depends on the rate at which acidifying compounds are deposited from the atmosphere, compared with the rate at which acid neutralizing capacity (ANC) is generated within the ecosystem (Driscoll et al., 2001).

Here we analyse how dry and wet deposition of sulfur species are distributed globally as a result of the two SG interventions. Table 2 and 3 summarize wet and dry deposition rates for the SG-COS and BG experiments, respectively, and they include the contribution of each species to the total deposition. In particular, in SG-COS the increase in COS fluxes produces both an

160   increase in sulfuric deposition, after its photolysis and oxidation to sulfuric acid, and in dry deposition of COS itself, as it is removed to the ground through uptake by vegetation and soils (Kettle et al., 2002).

The global distribution of COS deposition for the baseline case is shown in figure 6(a) while the increase in deposition from the SG-COS experiment is shown in figure 6(b). COS uptake by plants is concentrated mainly in the tropical rainforests of South America, Africa, and southeast Asia and boreal coniferous forests across North America, northern Europe, and northern

165   Asia. Uptake by soils occurs mainly in arid and semiarid regions, such as savanna regions in the northern and southern Africa and in the southwestern regions of North America, in the pampas of Argentina, in Australia, and in the steppes of central Asia (Kettle et al., 2002). Dry deposition of COS doesn't contribute to acid deposition and, currently, there is no information available on how different soils or ecosystems would be affected by higher local COS concentrations; therefore, we assumed that their uptake efficiency does not change. The robustness of this assumption will need to be studied.

170   The global distribution of SO_x deposition is also shown in figure 6. Panels (c) and (d) show dry and wet deposition, respectively, for the background case. Dry deposition maxima are localized in urban areas close to the source where the emitted sulfur dioxide is immediately oxidized, while wet deposition distribution depends both on sulfate concentration and precipitation.

Panels (e) and (f) show the total SO_x deposition change in SG-COS with respect to the baseline case, in absolute terms and as a percentage of the baseline case, and most of its increase is due to wet deposition (see tables 2 and 3, and see Tables S1-4

175   for a breakdown of global sources and sinks of sulfur species). In both figures, the distribution of deposition is more uniform over the globe with respect to the tropical injection of SO_2, except for the polar regions, because of the reduced precipitation rates. Consequently, figure 6 (f) shows a large increase in percent deposition in the polar region (17% in the Arctic, 8% in Antarctic) because of very low values in the baseline case. On the other hand, deposition change is close to zero in polluted regions.

180   Globally, the annual differences in deposition fluxes for all species compared to the background case amount to 8.3 ± 0.2 Tg-S/yr for SG-COS and 3.9 ± 0.2 Tg-S/yr for SG-SO2, which equates to an increase of 8.9 ± 0.3 % and 4.2 ± 0.3 %, respectively.
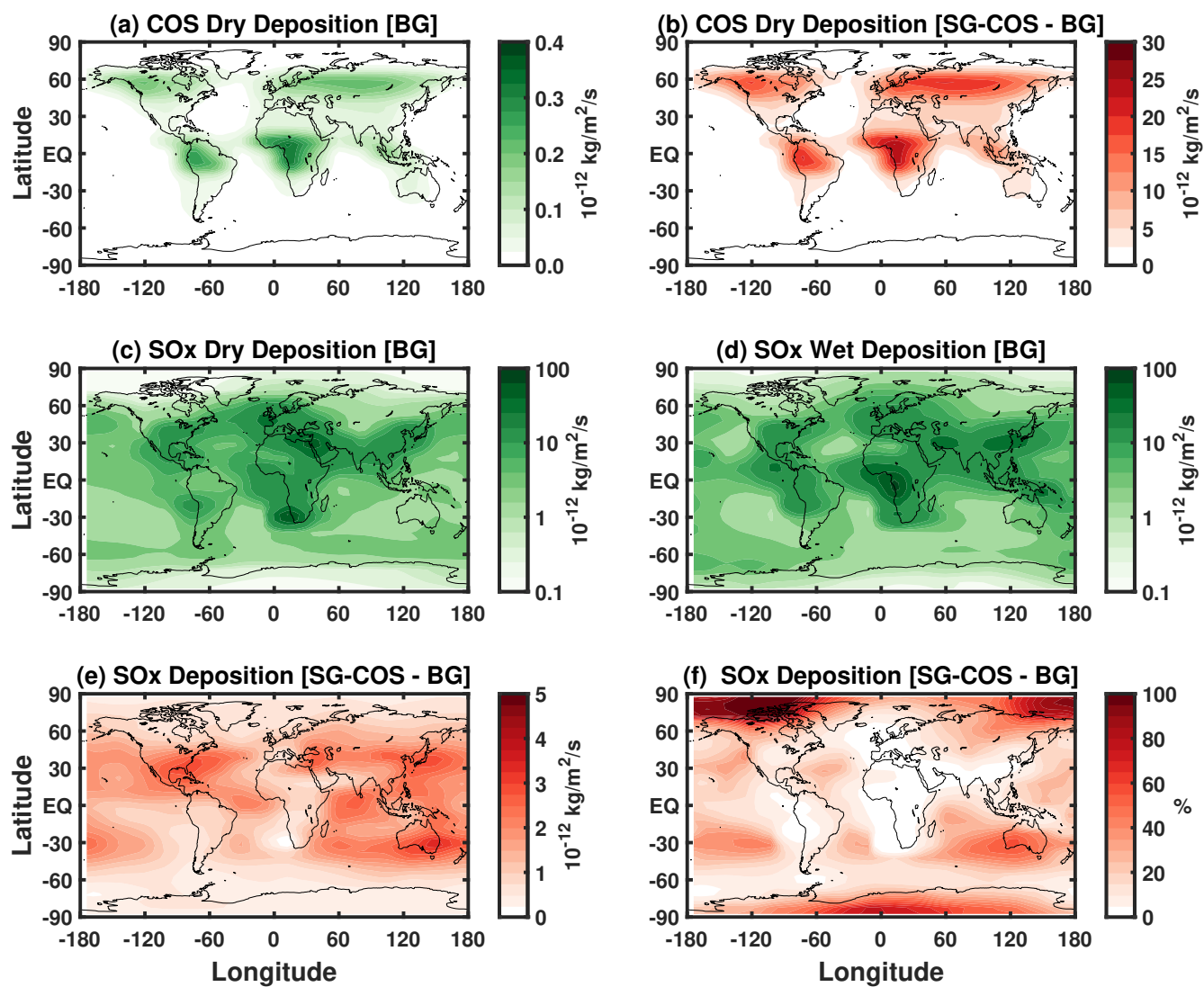
Figure 6. a) Surface dry deposition fluxes $(10^{-12}\,\mathrm{kg/m^2/s})$ of COS in the background case. b) Change in COS dry deposition fluxes in SG-COS compared to a). c) SO_x dry deposition fluxes $(10^{-12}\,\mathrm{kg/m^2/s})$ in the background case. d) SO_x dry deposition fluxes $(10^{-12}\,\mathrm{kg/m^2/s})$ in the background case. e) Change in SO_x total deposition fluxes in SG-COS compared to the background. f) as e) but in % of the background values.

4 Indirect effects

	BG	SG-COS	SG-SO2	SG-COS - BG	SG-SO2 - BG
COS [troposphere] (ppbv)	0.47±0.1	35.5±0.2	0.47±0.1	35.1±0.2	0.00±0.1
CH4 lifetime (yr)	8.72±0.13	9.83±0.18	9.78±0.20	1.11±0.13 [(+12.7±1.4) %]	1.06±0.17 [(+12.2±2.0) %]
H2O [stratosphere] (ppmv)	6.01±0.08	5.87±0.17	6.02±0.14	-0.14±0.11	0.01±0.08
O3 column (DU)	288.9±1.7	293.8±1.5	290.4±1.6	4.9±2.2	1.5±1.7

Table 4. Summary of calculated sulfate aerosol and cirrus ice globally-annually averaged quantities relevant for RF calculations (*i.e.*, optical depth at λ=0.55 μm and effective radius). Last two columns show the calculated SG changes with respect to the BG case [years 2046-2055].

	BG (W/m^2)	SG-COS (W/m^2)	SG-SO2 (W/m^2)	SG-COS - BG (%)	SG-SO2 - BG (%)
UVB	0.208±0.002	0.199±0.001	0.203±0.001	-4.3±0.6	-2.4±0.9
UVA	11.43±0.01	11.20±0.01	11.25±0.01	-2.0±0.1	-1.6±0.1

Table 5. Summary of calculated globally-annually averaged quantities of UVB and UVA at surface. Last two columns show the calculated SG percentage changes with respect to the BG case [years 2046-2055].

The simulated enhancement in the stratospheric aerosol layer would produce two main effects: an increased scattering of solar radiation, that in turn would reduce surface temperatures, and the local absorption of more near-infrared solar and terrestrial radiation, that would warm the stratospheric layer where the aerosols reside (as observed for volcanic eruptions, see Lacis et al., 1992; Labitzke and McCormick, 1992). Furthermore, the increase in the surface area density of the aerosols would affect the heterogeneous chemistry of ClO_x and NO_x with implications for ozone concentration and UV radiation at the surface (Tilmes et al., 2009, 2018b, 2021).

For SO_2, it has been shown that the combination of surface cooling, perturbation of stratospheric temperatures and changes in tropospheric ozone and in UV at the surface also affects methane lifetime (Visioni et al., 2017a). In this section we analyse the differences in these changes also for the SG-COS experiment.

Figure 7 shows the ozone changes in the two SG experiments with respect to the BG case. Panels (a) and (b) show the monthly total ozone column changes as a function of latitude. Close to the equator there is a small reduction in the overall

195 column, mostly due to a reduction in tropospheric ozone, as visible in panels (c) and (d), as a direct consequence of the surface cooling (Nowack et al., 2016). On the other hand, at higher latitudes an overall increase in the total column is observable due to an increase in stratospheric ozone. This is particularly evident closer to the poles.

During springtime months, there is some Antarctic ozone depletion, while in the Arctic a recovery of ozone is observable. In the Antarctic spring, the polar vortex is strengthened by the stratospheric heating in the tropics that affects the equator-to-

200 pole thermal wind balance (Visioni et al., 2020), resulting in greater confinement of cold air, that, in turn, enhances the ozone depletion by the polar stratospheric clouds (PSC). The tropical stratospheric heating is higher in SG-SO2 with respect to SG-COS as the aerosols are less confined (fig. S4). Consequently, the strengthening of polar vortex in SG-SO2 produces a higher ozone depletion. In the Arctic, on the other hand, PSC-related ozone loss is lower (Tilmes et al., 2018a), and the predominant effect is that from an acceleration of the BDC transporting ozone-rich air from lower latitudes.

205 Panels (c) and (d) show the annual mean of ozone mixing ratio percentage change as a function of altitude and latitude. In both SG experiments, negative changes below the tropopause are governed by the decrease in solar radiation which comes into play in the photo-dissociation reaction of NO_x as an ozone precursor (NO_2 + hν (λ < 420 nm) → NO + ^{3}O). Sunlight reduction also affects the O_3 photolysis, decreasing the ozone loss. Positive changes are due to the balance of the previous reactions and the increase of methane (see table 4) as a source of ozone in its oxidation chain, and mainly due to the decrease

210 of the tropospheric water vapour in a clean air environment (low NO_x), such as the tropics (Nowack et al., 2016; Xia et al., 2017b).

Above the tropopause, there is a negative ozone change in the lower stratosphere in both SG experiments, except for the Arctic region where we observe a small increase in the Arctic lowermost stratosphere in both cases. The key drivers of stratospheric ozone change are the increase in heterogeneous reactions, as a result of the enhancement of stratospheric aerosols, and

215 the perturbation of the dynamics governing ozone transport.

Negative ozone changes correspond to the region where the SAD reaches its maximum values (fig. 5 (d) and (f)): between 10-20 km in the polar regions for SG-COS and mainly between 15-25 km at tropics for SG-SO2. The increase of the SAD enhances heterogeneous chemistry and results in denitrification via hydrolysis of dinitrogen pentoxide (N_2O_5 + H_2O $\xrightarrow{M}$ 2HNO$_3$). The loss of NO_x decreases the rate of ozone depletion through its catalytic cycle. Whereas in the mid-stratosphere,

220 where the cycles of chlorine (ClO_x) and bromine (BrO_x) are dominant, there is an increase in ozone loss since reduction of NO_x, that normally bounds chlorine ($ClONO_2$), allows ClO to destroy more ozone (Tilmes et al., 2018b; Grant et al., 1992).

At low latitudes, stratospheric ozone concentration is also driven by change of tropical upwelling (Visioni et al., 2021): the reduction of tropical upwelling of ozone-poor air coming from the lowermost stratosphere leads to higher ozone concentration at altitudes of about 20-22 km (Tilmes et al., 2018b).

225 Figure S5 (e) shows the change of tropical upwelling in relation to change of the residual vertical velocity (w*) with respect to the baseline case. Negative w* anomalies in SG-COS mean weaker tropical upwelling as consequence of tropospheric cooling. In SG-SO2, the highest concentration of absorbing aerosols leads to positive w* above 20 km due to the local warming but this doesn't affect the transport of ozone-poor air from the lower layers.

Above the discussed altitudes, there is a net ozone production in both SG experiments, with an higher increase of ozone
230   mixing ration in SG-COS experiment with respect to SG-SO2, especially in the extra-tropical region. Ozone depletion at these
altitudes is mainly controlled by the catalytic cycle of NO_x, that is inhibited by the denitrification process due to heterogeneous
reactions on aerosols.

Globally, the annually-averaged ozone column increases of 4.9 and 1.5 DU for SG-COS and SG-SO2, respectively (table 4).
The stratospheric ozone increase affects UVB at the surface due to its photodissociation, while aerosol could affect UVA
235   radiation by scattering processes: the projected changes are shown in figure 8 for both UVA and UVB. We estimated these
changes using TUV (from https://www2.acom.ucar.edu/modeling/tropospheric-ultraviolet-and-visible-tuv-radiation-model),
using in input our model latitudinal and monthly values for the period (2046-2055) for aerosol optical depth, total ozone
column, climatological cloud cover and surface albedo.

In both SG experiments, the negative changes of UVB radiation at surface, except in the Antarctic region, are related to the
240   variation in stratospheric ozone. as well as the interannual variation that increase towards the poles, due to the seasonal variation
of ozone, as discussed before. UVA decrease is everywhere negative in both SG experiments. In particular, the correlation
between UVA change and particles scattering is evident if we compare this latitudinal distribution with the stratospheric AOD
of figure 3(a). The globally averaged UVB and UVA changes at surface are summarized in table 5.

Methane is an indirect source of tropospheric ozone (West and Fiore, 2005), and it is also a greenhouse gas. Knowing its
245   variation is fundamental to understand the final contribution to the radiative forcing that one would wish to achieve with this
geoengineering method. From table 4, we measure a global increase in methane lifetime of 12.7% in SG-COS and 12.2% in
SG-SO2, which we can identify in the increase in methane itself. The reason for the increase in methane is to be found in
the behaviour of the hydroxyl radical (OH), as the main sink of methane is the oxidation reaction with OH: decrease of OH
means an increase of methane lifetime. As discussed by Visioni et al. (2017b), mechanisms that cause an increase in OH are
250   as follows: (a) surface cooling lessens the amount of tropospheric water vapor and inhibits the temperature-dependent reaction
of $NO + O_3$; (b) decrease of tropospheric UV, due to enhancement of ozone and scattering radiation, reduce $O(^1D)$ that takes
part of the reaction $O(^1D) + H_2O \rightarrow 2\,OH$; (c) increase of SAD enhances heterogeneous chemistry reducing the amount of
NO_x ($NO + HO_2$, $NO + RO_2$); (d) increase of tropical lower stratosphere temperature (TTL) that regulates the stratosphere-
troposphere exchange, which can be positive or negative depending on the net result of the superimposed species (CH_4, NO_y,
255   O_3, SO_4) in the extratropical upper troposphere-lower stratosphere (UTLS).

The warming of the TTL is shown in figure S5 (d): in SG-SO2, larger particles confined in the tropical region produce a
greater warming of the TTL with respect to smaller ones distributed all over the globe in SG-COS. The role of dimensions and
distributions of aerosols in stratospheric warming is confirmed by the heating rates, as shown in figure S4.
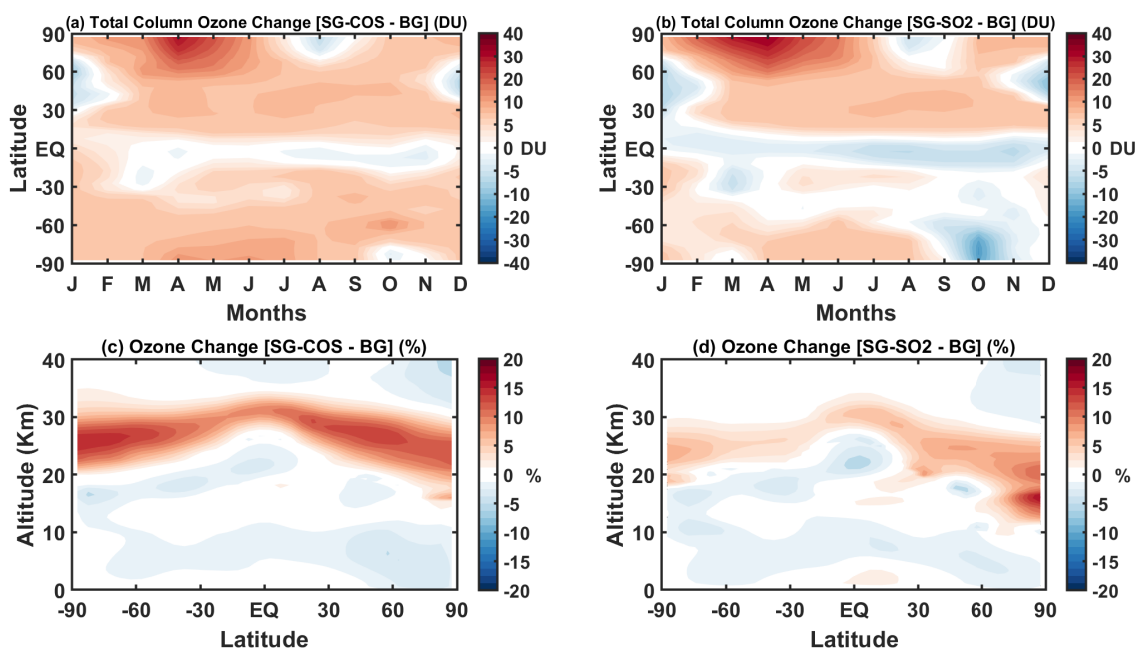
Figure 7. a,b) Monthly mean zonal values of SG ozone total column changes (DU) with respect to the BG case for SG-COS and SG-SO2 respectively. c, d) ozone mixing ratio percent changes with respect to the BG case. All quantities are annually averaged over the years 2046-2055.

5 Radiative forcing

Total RF (W/m^2)	SW	LW	NET
SG-COS	-1.47±0.12	+0.18±0.25	-1.29±0.13
SG-SO2	-1.57±0.10	-0.13±0.23	-1.70±0.13

Table 6. Globally-annually averaged total RF of sulfate aerosols and greenhouse gases for the two SG experiments with respect to BG (shortwave, longwave and net) (W/m^2) [years 2046-2055].

260 The ULAQ-CCM radiative transfer module calculates online the radiative forcing due to aerosols, greenhouse gases (GHGs), and low and high clouds. The effects of single components have been estimated offline for both shortwave (SW) and longwave (LW) with the same radiative transfer core, for sulfate aerosols, clouds, COS, CH$_4$, stratospheric H$_2$O, stratospheric and tropospheric O$_3$ in order to properly separate the contributions.

Tables S7 and S8 summarise the individual contributions of GHGs changes for SG-COS and SG-SO2, respectively. Similar
265 increases of methane in both SG experiments produce the same positive LW RF; the TTL warming (which results in an
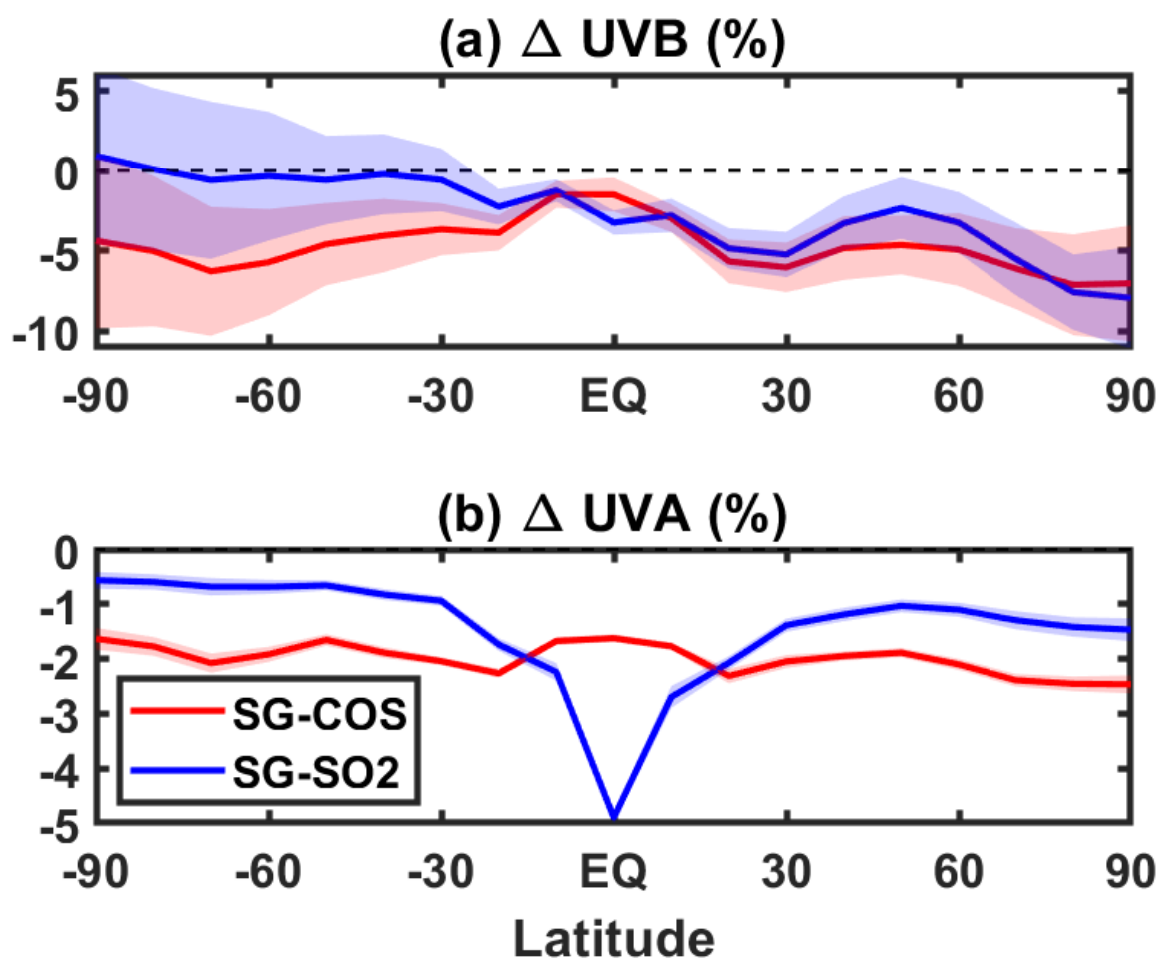
Figure 8. Mean zonal UVB and UVA percent changes at surface with respect to BG case (panels a and b, respectively) in SG-COS (red) and SG-SO2 (blue). All quantities are annually averaged over the years 2046-2055.

increase in stratospheric water vapor), results in a small but positive contribution from H_2O in SG-SO2. Contributions from both stratospheric and tropospheric O_3 changes have also been estimated, but are negligible.

In SG-COS, obviously, the increase of COS concentration, which is a GHG, must be taken into account. We estimated its contribution to RF based on the definition of global warming potential (GWP) on a mass/mass basis as in Bruhl et al. (2012) for a time horizons of 30 years (2021-2050). GWP can be approximated as follows by the expression of Roehl et al. (1995), assuming that the perturbation of the radiation balance of the Earth by greenhouse gases COS and CO_2 decays exponentially after a pulse emission for a time horizon ΔT.

$$GWP_{\Delta t} \simeq \frac{RF_{COS}}{RF_{CO_2}} \times \frac{\tau_{COS}}{\tau_{CO_2}} \times \frac{1 - exp\frac{-\Delta t}{\tau_{COS}}}{1 - exp\frac{-\Delta t}{\tau_{CO_2}}} \tag{1}$$

We assumed an overall lifetime of τ_{COS}=3.8 yr and τ_{CO_2}=75 yr, and the radiative forcing of 1 kg of COS relative to 1 kg of CO_2 added to the present atmosphere (RF_{COS}/RF_{CO_2}) is 724 (Brühl and Crutzen, 1988). This results in a GWP of 111. For our time period, the mass of COS and CO_2 added to the atmosphere (Δm) is 1.97 10^{12} kg of COS and 1.23 10^{15} kg of CO_2. Therefore, the COS radiative forcing can be calculated as:

$$RF_{COS} = GWP_{\Delta t} \times RF_{CO_2} \times \frac{\Delta m_{COS}}{\Delta m_{CO_2}} \tag{2}$$

where RF_{CO_2} in RCP6.0 is estimated to be 0.83 W/m^2 considering an increase of 68.5 ppm from a baseline of 409.2 ppm. Overall, this results in a radiative forcing from the COS increase of 0.17 W/m^2.

The main contributions of sulfate aerosols and clouds are summarised in tables S5 and S6 for SG-COS and SG-SO2, respectively. Globally, the estimated values are similar for the Clear-Sky SW and LW forcing from the sulfate aerosols: in terms of the latitudinal distribution, however, SG-SO2 presents a peak in the tropics whereas the forcing from SG-COS is much more latitudinally even.

The reduction in optical depth from cirrus clouds (see table 1) produced by the aerosols (Kuebbeler et al., 2012; Visioni et al., 2018a) results in a net negative radiative forcing given by the balance between the reduction of reflected solar radiation, resulting in a positive RF in the shortwave (SW) and the decrease of trapped planetary radiation, which reduces the contribution to the greenhouse effect with a negative RF in the longwave (LW). In the SG-COS case, at the equator the positive RF from the thinning locally cancels out the direct forcing from the aerosol (9 and fig. S6).

Table 6 summarises the total contribution of sulfate aerosols and greenhouse gases under All-Sky conditions.

6   Technical feasibility of SG through COS emissions

We briefly discuss here the technical feasibility of the approach described in this paper, as related to the increase of surface COS emissions (for SO_2 injections, see for instance Smith and Wagner, 2018).

Patent number 3,409,399 (1968) has developed a method for high yield synthesis of COS (93.2-96.6%):
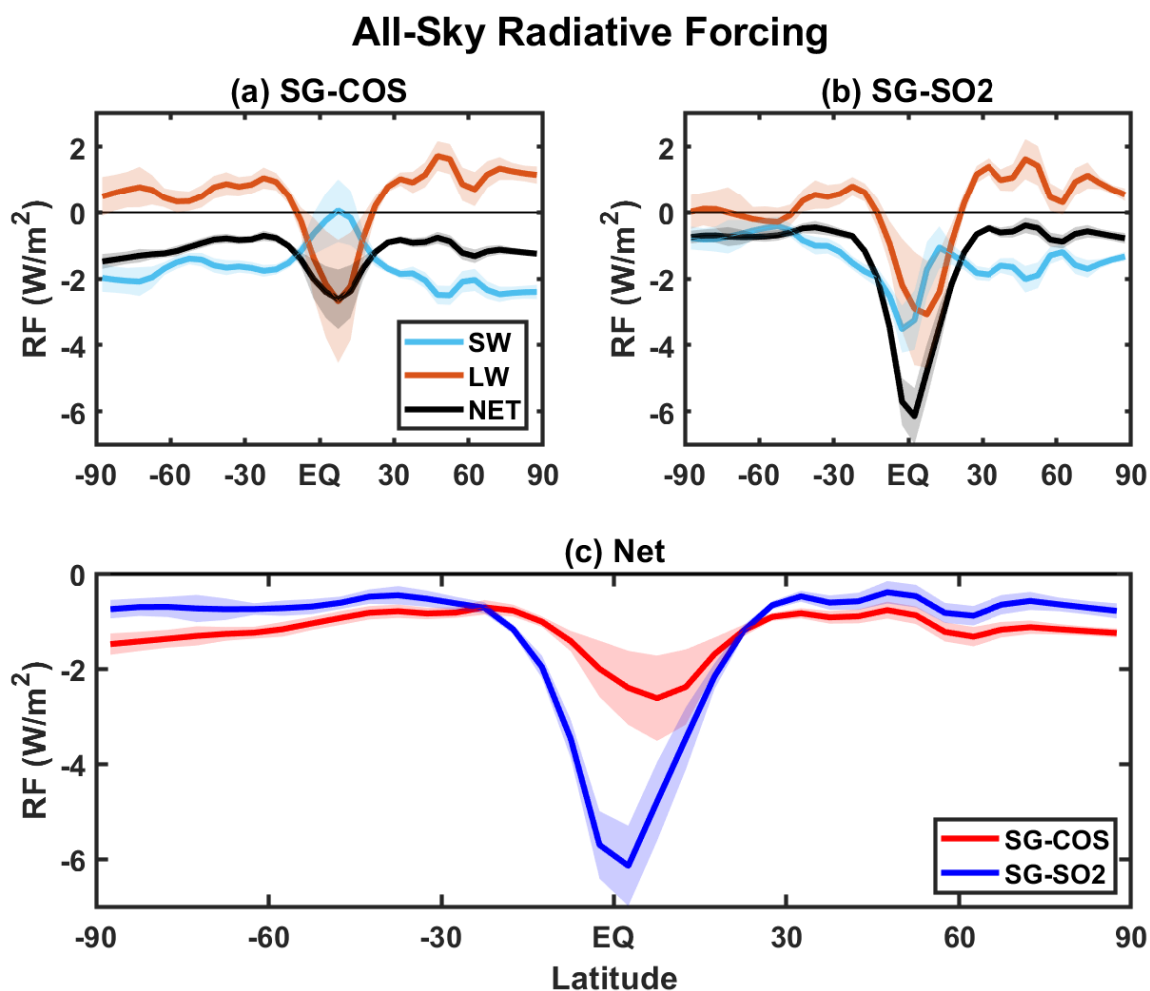
Figure 9. a-b) Mean zonal shortwave (cyan), longwave (orange), and net (black) radiative forcing (in W/m^2) in SG-COS and SG-SO2 respectively. c) Comparison of the net radiative forcings from SG-COS (red) and SG-SO2 (blue). All quantities are annually averaged over the years 2046-2055. Shadings in all panels represent 1 standard deviation in the interannual variability.

295    $CO_2 + CS_2 \xrightarrow{\;100-600^\circ C\;} 2COS$
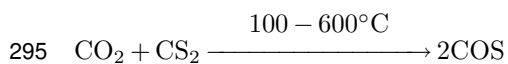
CO_2 is abundant even in concentrated (90%+) streams, from various natural and industrial sources, particularly with co-operation from states or industries. For example, capturing flue gas from coal-fired power plants is an established technology and may yield over 90% CO_2 (Wang et al., 2013). CS_2 is produced via numerous means, perhaps the easiest being from coke

300   (carbon) and molten sulfur:

$C + 2S \xrightarrow{\;\text{high temperature}\;} CS_2$
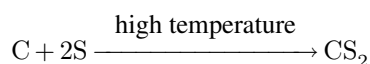
Approximately 1 million tons of CS_2 is produced per year (Madon and Strickland-Constable, 1958), with China consuming approximately half of the global production of CS_2 for rayon manufacturing. CS_2 is highly unstable and is flammable in air. It

305   is also toxic at low concentrations (10 ppm).

Given the reactions above, about 0.5 Tg of S will produce 0.94 Tg of COS: this amounts to 0.16 Tg of C (coke) and 0.55 Tg of molten sulfur. In the last decade, approximately 70 Tg of sulfur were produced worldwide, so this would constitute an increase in S production of 0.8%. The price varied between $50 and $200 per ton, leading to an annual cost of approximately $25-100 million. Worldwide production of coke was around 640 Tg, so this increase in production is negligible. The price of

310   coke varies between $50 and $100 per ton, leading to an annual cost of approximately $8-16 million.

To this we would have to add the cost of CO_2, as well as the production and energy costs. Considering an estimate of $400 million per year for each Tg of S between CO_2 and production and energy cost, and assuming an effort shared between 1000 locations, this would add up to $400.000 per location per year per each Tg of S. The overall cost is roughly of the same order of magnitude as that in Smith and Wagner (2018) for a stratospheric aerosol deployment at ~ 20 km of injection (so different

315   from the injection set-up in our study for SG-SO2), but without the need to develop a new aircraft-based delivery system.

7   Conclusions

We have presented here the results of a modeling experiment with the aim of producing an optically thick cloud of sulfate aerosols in the stratosphere without the injection of sulfate precursors directly in the stratosphere, but rather using increased surface emissions of carbonyl sulfide (COS). The low reactivity of COS in the troposphere, where it is not reactive and where

320   it is predominantly absorbed by some soils and by plants, allows for a large portion of its emissions to reach the stratosphere, where it is turned into sulfate aerosols by photo-dissociation and oxidation.

We compare the results obtained with an increased emission of 40 Tg-S/yr (roughly 400 times more than the background emissions) with those from a 4 Tg-S/yr injection of SO_2 in the stratosphere as prescribed in previous experiments (Kravitz

et al., 2011; Visioni et al., 2017a). Both experiments result in a similar global optical depth from the produced stratospheric
aerosols (~ 0.07), but with different latitudinal distributions: for SO_2, as previously observed in various modeling experiments,
equatorial injections result in an increased concentration of aerosols in the tropical stratosphere that tends to overcool the tropics
and undercool the high latitudes (Kravitz et al., 2018; Jiang et al., 2019), while also reducing the efficacy of the back-scattering
from the aerosols due to the increased size of the particles (Visioni et al., 2018c). On the other hand, with COS emissions the
uniform mixing of the gas allows for a more uniform distribution of the produced aerosols in the stratosphere, resulting in
increased optical depth also at very high latitude.

The differences in distribution and size of the particles result in different changes to the composition of the atmosphere:
smaller particles absorb and heat the stratosphere less, thus resulting in fewer dynamical changes. From a chemical perspective, stratospheric ozone would be impacted differently from the two geoengineering schemes. For SO_2 injections, previous
studies have shown that the overall effect is the result of a combination of various dynamical and chemical factors that behave
differently depending on the latitude and altitude of the aerosols.

At low latitudes the increase in lower stratospheric water vapor produced by the warming of the tropopause layer enhances
the halogen-driven destruction of ozone in the lower stratosphere (Tilmes et al., 2018b) due to NO_x depletion. This effect is
balanced by reduced ozone destruction in the middle stratosphere due to the slowing down of the NO_x cycle produced by
enhanced heterogeneous chemistry (Pitari et al., 2014; Richter et al., 2017; Franke et al., 2020).

Overall, in the case of COS emissions the further increase in SAD produced by smaller particles increases the inhibition of
the ozone cycles in the middle stratosphere, resulting in a net increase in stratospheric ozone and thus in a larger decrease of
UV radiation at the surface. Similarly, the larger sulfate burden at high latitudes produces further ozone recovery and thus less
UV radiation also at the poles for the COS case.

Our results point to the feasibility of surface emissions of COS as a possible substitute to stratospheric SO_2 (or other sulfate
precursors) injections to produce stratospheric sulfate aerosols. This would sidestep the problem of deploying methods not
already available to bring the sulfate at those altitudes, including development of novel aircraft (Bingaman et al., 2020).

Since COS is already a byproduct of human activities, it might be possible to devise methods of mass-production of the
required quantities that may be cheaper than the known proposed methods (Smith et al., 2020).

Overall, there are some weak points in a geoengineering strategy using COS compared to SO_2 that need to be addressed.
First, it necessitates a larger amount of emissions to achieve the same global stratospheric AOD, resulting in larger amounts of
deposition. It would be less easily scalable, and both deployment and phase-out, as we have shown, would require a much longer
time-frame compared to the almost instantaneous effect produced by SO_2 injections. Considering the dangers to ecosystems
presented by a too fast deployment or termination of sulfate geoengineering (Trisos et al., 2018), this might not actually be a
large drawback, but it does remove the possibility of rapidly "regulating" the necessary amount of stratospheric sulfate in case
of changes in strategy or external conditions (such as a Pinatubo-like volcanic eruption; Laakso et al., 2016). Furthermore, the
mixing happening in the troposphere would not allow any control in the latitudinal or seasonal distribution of the resulting
aerosols, as proposed elsewhere (MacMartin et al., 2017; Dai et al., 2018; Visioni et al., 2019).

Clearly, this study is intended to be just a pilot study of this newly proposed method, and further simulations with other climate models, possibly with a coupled ocean and interactive land model, to determine the surface response, are needed. The

360 agreement between the baseline results presented here and the information present in the literature point to a robustness of our results, but further studies are required to understand different aspects of the climate response: for instance, studies would need to investigate the possible response of vegetation and soils to the increased concentration of COS in the troposphere, and if the efficacy of the sinks would change due to shifts in temperature and precipitation produced by both climate change and the intervention.

365 While toxic levels of COS concentrations are many orders of magnitude larger than the one achieved in our simulations (Kilburn and Warshaw, 1995; Bartholomaeus and Haritos, 2006), the effects of prolonged exposure to lower concentrations will have to be assessed. Estimations of the tropospheric radiative effect would also need to be refined to make sure that it is not larger than previously estimated, reducing the efficacy of the aerosol-induced cooling. Overall, however, the results obtained in this work show that, as a geoengineering technique, the surface emission of carbonyl sulfide should be further studied and

370 considered by the scientific community as a possible alternative to the others already studied in the literature.

Data availability. Data used in this work will be made available through the Cornell eCommons platform before publication.

Author contributions. DV and GP devised the study. IQ ran the simulations, analysed the results, produced the figures and wrote the manuscript with the assistance of DV. BK wrote Section 6 and contributed to the final draft of the manuscript.

Competing interests. The authors declare no competing interests

375 *Acknowledgements.* Support for B.K. was provided in part by the National Science Foundation through agreement CBET-1931641, the Indiana University Environmental Resilience Institute, and the *Prepared for Environmental Change* Grand Challenge initiative. Support for D.V. was provided by the Atkinson Center for a Sustainable Future at Cornell University.

References

Barkley, M. P., Palmer, P. I., Boone, C. D., Bernath, P. F., and Suntharalingam, P.: Global distributions of carbonyl sulfide in the upper troposphere and stratosphere, Geophysical Research Letters, 35, https://doi.org/https://doi.org/10.1029/2008GL034270, 2008.

Bartholomaeus, A. and Haritos, V.: Review of the toxicology of carbonyl sulfide, a new grain fumigant, Food and chemical toxicology : an international journal published for the British Industrial Biological Research Association, 43, 1687–701, https://doi.org/10.1016/j.fct.2005.06.016, 2006.

Bingaman, D. C., Rice, C. V., Smith, W., and Vogel, P.: A Stratospheric Aerosol Injection Lofter Aircraft Concept: Brimstone Angel, in: AIAA Scitech 2020 Forum, AIAA SciTech Forum, American Institute of Aeronautics and Astronautics, https://doi.org/10.2514/6.2020-0618, 2020.

Bruhl, C., Lelieveld, J., Crutzen, P. J., and Tost, H.: The role of carbonyl sulphide as a source of stratospheric sulphate aerosol and its impact on climate, Atmospheric Chemistry and Physics, 12, 1239–1253, 2012.

Brühl, C. and Crutzen, P. J.: Scenarios of possible changes in atmospheric temperatures and ozone concentrations due to man's activities, estimated with a one-dimensional coupled photochemical climate model, Climate Dynamics, 2, 173–203, https://doi.org/10.1007/BF01053474, 1988.

Budyko, M. I.: The Climate of the Future, American Geophysical Union, https://doi.org/10.1002/9781118665251.ch7, 1978.

Crutzen, P. J.: The possible importance of CSO for the sulfate layer of the stratosphere, Geophysical Research Letters, 3, 73–76, https://doi.org/https://doi.org/10.1029/GL003i002p00073, 1976.

Crutzen, P. J.: Albedo Enhancement by Stratospheric Sulfur Injections: A Contribution to Resolve a Policy Dilemma?, Climatic Change, 77, 211–220, https://doi.org/10.1007/s10584-006-9101-y, 2006.

Dai, Z., Weisenstein, D. K., and Keith, D. W.: Tailoring Meridional and Seasonal Radiative Forcing by Sulfate Aerosol Solar Geoengineering, Geophysical Research Letters, 45, 1030–1039, https://doi.org/10.1002/2017GL076472, 2018.

Driscoll, C. T., Lawrence, G. B., Bulger, A. J., Butler, T. J., Cronan, C. S., Eagar, C., Lambert, K. F., Likens, G. E., Stoddard, J. L., and Weathers, K. C.: Acidic Deposition in the Northeastern United States: Sources and Inputs, Ecosystem Effects, and Management Strategies: The effects of acidic deposition in the northeastern United States include the acidification of soil and water, which stresses terrestrial and aquatic biota, BioScience, 51, 180–198, https://doi.org/10.1641/0006-3568(2001)051[0180:ADITNU]2.0.CO;2, 2001.

Eastham, S. D., Weisenstein, D. K., Keith, D. W., and Barrett, S. R.: Quantifying the impact of sulfate geoengineering on mortality from air quality and UV-B exposure, Atmospheric Environment, 187, 424 – 434, https://doi.org/https://doi.org/10.1016/j.atmosenv.2018.05.047, 2018.

Eichinger, R., Dietmuller, S., Garny, H., Sacha, P., Birner, T., Bonisch, H., Pitari, G., Visioni, D., Stenke, A., Rozanov, E., Revell, L., Plummer, D. A., Jockel, P., Oman, L., Deushi, M., Kinnison, D. E., Garcia, R., Morgenstern, O., Zeng, G., Stone, K. A., and Schofield, R.: The influence of mixing on the stratospheric age of air changes in the 21st century, Atmospheric Chemistry and Physics, 19, 921–940, 2019.

English, J. M., Toon, O. B., and Mills, M. J.: Microphysical simulations of sulfur burdens from stratospheric sulfur geoengineering, Atmospheric Chemistry and Physics, 12, 4775–4793, 2012.

Eyring, V., Butchart, N., Waugh, D. W., Akiyoshi, H., Austin, J., Bekki, S., Bodeker, G. E., Boville, B. A., Brühl, C., Chipperfield, M. P., Cordero, E., Dameris, M., Deushi, M., Fioletov, V. E., Frith, S. M., Garcia, R. R., Gettelman, A., Giorgetta, M. A., Grewe, V., Jourdain, L., Kinnison, D. E., Mancini, E., Manzini, E., Marchand, M., Marsh, D. R., Nagashima, T., Newman, P. A., Nielsen, J. E., Pawson, S., Pitari,

415   G., Plummer, D. A., Rozanov, E., Schraner, M., Shepherd, T. G., Shibata, K., Stolarski, R. S., Struthers, H., Tian, W., and Yoshiki, M.: Assessment of temperature, trace species, and ozone in chemistry-climate model simulations of the recent past, Journal of Geophysical Research, 111, D22 308, https://doi.org/10.1029/2006JD007327, 2006.

Franke, H., Niemeier, U., and Visioni, D.: Differences in the QBO response to stratospheric aerosol modification depending on injection strategy and species, Atmospheric Chemistry and Physics Discussions, 2020, 1–29, https://doi.org/10.5194/acp-2020-1104, 2020.

420   Grant, W., Fishman, J., Browell, E., Brackett, V., Nganga, D., Minga, A., Cros, B., Veiga, R. E., Butler, C., Fenn, M., and Nowicki, G.: Observations of reduced ozone concentrations in the tropical stratosphere after the eruption of Mt. Pinatubo, Geophysical Research Letters, 19, 1109–1112, 1992.

Jiang, J., Cao, L., MacMartin, D. G., Simpson, I. R., Kravitz, B., Cheng, W., Visioni, D., Tilmes, S., Richter, J. H., and Mills, M. J.: Stratospheric Sulfate Aerosol Geoengineering Could Alter the High-Latitude Seasonal Cycle, Geophysical Research Letters, 46, 14 153–
425   14 163, https://doi.org/10.1029/2019GL085758, 2019.

Kettle, A. J., Kuhn, U., von Hobe, M., Kesselmeier, J., and Andreae, M. O.: Global budget of atmospheric carbonyl sulfide: Temporal and spatial variations of the dominant sources and sinks, Journal of Geophysical Research: Atmospheres, 107, ACH 25–1–ACH 25–16, https://doi.org/https://doi.org/10.1029/2002JD002187, 2002.

Khalil, M. and Rasmussen, R.: Global sources, lifetimes and mass balances of carbonyl sulfide (OCS) and carbon disulfide (CS2) in the
430   earth's atmosphere, Atmospheric Environment (1967), 18, 1805–1813, 1984.

Kilburn, K. H. and Warshaw, R. H.: Hydrogen Sulfide and Reduced-Sulfur Gases Adversely Affect Neurophysiological Functions, Toxicology and Industrial Health, 11, 185–197, 1995.

Kravitz, B., Robock, A., Boucher, O., Schmidt, H., Taylor, K. E., Stenchikov, G., and Schulz, M.: The Geoengineering Model Intercomparison Project (GeoMIP), Atmospheric Science Letters, 12, 162–167, https://doi.org/10.1002/asl.316, 2011.

435   Kravitz, B., Rasch, P. J., Wang, H., Robock, A., Gabriel, C., Boucher, O., Cole, J. N. S., Haywood, J., Ji, D., Jones, A., Lenton, A., Moore, J. C., Muri, H., Niemeier, U., Phipps, S., Schmidt, H., Watanabe, S., Yang, S., and Yoon, J.-H.: The climate effects of increasing ocean albedo: an idealized representation of solar geoengineering, Atmospheric Chemistry and Physics, 18, 13 097–13 113, https://doi.org/10.5194/acp-18-13097-2018, 2018.

Kuai, L., Worden, J. R., Campbell, J. E., Kulawik, S. S., Li, K.-F., Lee, M., Weidner, R. J., Montzka, S. A., Moore, F. L., Berry, J. A., Baker,
440   I., Denning, A. S., Bian, H., Bowman, K. W., Liu, J., and Yung, Y. L.: Estimate of carbonyl sulfide tropical oceanic surface fluxes using Aura Tropospheric Emission Spectrometer observations, Journal of Geophysical Research: Atmospheres, 120, 11,012–11,023, https://doi.org/https://doi.org/10.1002/2015JD023493, 2015.

Kuebbeler, M., Lohmann, U., and Feichter, J.: Effects of stratospheric sulfate aerosol geo-engineering on cirrus clouds, Geophysical Research Letters, 39, https://doi.org/10.1029/2012GL053797, l23803, 2012.

445   Kuhn, U. and Kesselmeier, J.: Environmental variables controlling the uptake of carbonyl sulfide by lichens, Journal of Geophysical Research: Atmospheres, 105, 26 783–26 792, https://doi.org/https://doi.org/10.1029/2000JD900436, 2000.

Laakso, A., Kokkola, H., Partanen, A.-I., Niemeier, U., Timmreck, C., Lehtinen, K. E. J., Hakkarainen, H., and Korhonen, H.: Radiative and climate impacts of a large volcanic eruption during stratospheric sulfur geoengineering, Atmospheric Chemistry and Physics, 16, 305–323, https://doi.org/10.5194/acp-16-305-2016, 2016.

450   Labitzke, K. and McCormick, M. P.: Stratospheric temperature increases due to Pinatubo aerosols, Geophysical Research Letters, 19, 207–210, https://doi.org/10.1029/91GL02940, 1992.

Lacis, A., Hansen, J., and Sato, M.: Climate forcing by stratospheric aerosols, Geophysical Research Letters, 19, 1607–1610, https://doi.org/https://doi.org/10.1029/92GL01620, 1992.

Lamarque, J.-F., Dentener, F., McConnell, J., Ro, C.-U., Shaw, M., Vet, R., Bergmann, D., Cameron-Smith, P., Dalsoren, S., Doherty, R., Faluvegi, G., Ghan, S. J., Josse, B., Lee, Y. H., MacKenzie, I. A., Plummer, D., Shindell, D. T., Skeie, R. B., Stevenson, D. S., Strode, S., Zeng, G., Curran, M., Dahl-Jensen, D., Das, S., Fritzsche, D., and Nolan, M.: Multi-model mean nitrogen and sulfur deposition from the Atmospheric Chemistry and Climate Model Intercomparison Project (ACCMIP): evaluation of historical and projected future changes, Atmospheric Chemistry and Physics, 13, 7997–8018, https://doi.org/10.5194/acp-13-7997-2013, 2013.

Lee, C.-L. and Brimblecombe, P.: Anthropogenic contributions to global carbonyl sulfide, carbon disulfide and organosulfides fluxes, Earth-Science Reviews, 160, 1–18, https://doi.org/https://doi.org/10.1016/j.earscirev.2016.06.005, 2016.

Lockley, A., MacMartin, D., and Hunt, H.: An update on engineering issues concerning stratospheric aerosol injection for geoengineering, Environmental Research Communications, 2, 082 001, 2020.

MacMartin, D. G., Kravitz, B., Mills, M. J., Tribbia, J. J., Tilmes, S., Richter, J. H., Vitt, F., and Lamarque, J.-F.: The Climate Response to Stratospheric Aerosol Geoengineering Can Be Tailored Using Multiple Injection Locations, Journal of Geophysical Research: Atmospheres, 122, 12,574–12,590, https://doi.org/10.1002/2017jd026868, 2017.

Madon, H. N. and Strickland-Constable, R. F.: Production of CS2, Industrial & Engineering Chemistry, 50, 1189–1192, 1958.

Madronich, S., Tilmes, S., Kravitz, B., MacMartin, D. G., and Richter, J. H.: Response of surface ultraviolet and visible radiation to stratospheric SO2 injections, Atmosphere, 9, https://doi.org/10.3390/atmos9110432, 2018.

Meinshausen, M., Smith, S. J., Calvin, K., Daniel, J. S., Kainuma, M. L. T., Lamarque, J.-F., Matsumoto, K., Montzka, S. A., Raper, S. C. B., Riahi, K., Thomson, A., Velders, G. J. M., and van Vuuren, D. P. P.: The RCP greenhouse gas concentrations and their extensions from 1765 to 2300, Climatic Change, 109, 213, 2011.

Morgenstern, O., Giorgetta, M. A., Shibata, K., Eyring, V., Waugh, D. W., Shepherd, T. G., Akiyoshi, H., Austin, J., Baumgaertner, A. J. G., Bekki, S., Braesicke, P., Brühl, C., Chipperfield, M. P., Cugnet, D., Dameris, M., Dhomse, S., Frith, S. M., Garny, H., Gettelman, A., Hardiman, S. C., Hegglin, M. I., Jöckel, P., Kinnison, D. E., Lamarque, J.-F., Mancini, E., Manzini, E., Marchand, M., Michou, M., Nakamura, T., Nielsen, J. E., Olivié, D., Pitari, G., Plummer, D. A., Rozanov, E., Scinocca, J. F., Smale, D., Teyssèdre, H., Toohey, M., Tian, W., and Yamashita, Y.: Review of the formulation of present-generation stratospheric chemistry-climate models and associated external forcings, Journal of Geophysical Research, 115, D00M02, https://doi.org/10.1029/2009JD013728, 2010.

Morgenstern, O., Stone, K. A., Schofield, R., Akiyoshi, H., Yamashita, Y., Kinnison, D. E., Garcia, R. R., Sudo, K., Plummer, D. A., Scinocca, J., Oman, L. D., Manyin, M. E., Zeng, G., Rozanov, E., Stenke, A., Revell, L. E., Pitari, G., Mancini, E., Di Genova, G., Visioni, D., Dhomse, S. S., and Chipperfield, M. P.: Ozone sensitivity to varying greenhouse gases and ozone-depleting substances in CCMI-1 simulations, Atmospheric Chemistry and Physics, 18, 1091–1114, https://doi.org/10.5194/acp-18-1091-2018, 2018.

Mu, Y., Geng, C., Wang, M., Wu, H., Zhang, X., and Jiang, G.: Photochemical production of carbonyl sulfide in precipitation, Journal of Geophysical Research: Atmospheres, 109, https://doi.org/https://doi.org/10.1029/2003JD004206, 2004.

Neale, R. B., Richter, J., Park, S., Lauritzen, P. H., Vavrus, S. J., Rasch, P. J., and Zhang, M.: The Mean Climate of the Community Atmosphere Model (CAM4) in Forced SST and Fully Coupled Experiments, Journal of Climate, 26, 5150 – 5168, 2013.

Nowack, P. J., Abraham, N. L., Braesicke, P., and Pyle, J. A.: Stratospheric ozone changes under solar geoengineering: implications for UV exposure and air quality, Atmospheric Chemistry and Physics, 16, 4191–4203, https://doi.org/10.5194/acp-16-4191-2016, 2016.

Orbe, C., Yang, H., Waugh, D. W., Zeng, G., Morgenstern, O., Kinnison, D. E., Lamarque, J.-F., Tilmes, S., Plummer, D. A., Scinocca, J. F., Josse, B., Marecal, V., Jöckel, P., Oman, L. D., Strahan, S. E., Deushi, M., Tanaka, T. Y., Yoshida, K., Akiyoshi, H., Yamashita, Y., Stenke,

490   A., Revell, L., Sukhodolov, T., Rozanov, E., Pitari, G., Visioni, D., Stone, K. A., Schofield, R., and Banerjee, A.: Large-scale tropospheric transport in the Chemistry–Climate Model Initiative (CCMI) simulations, Atmospheric Chemistry and Physics, 18, 7217–7235, 2018.

Pitari, G., Mancini, E., Rizi, V., and Shindell, D. T.: Impact of Future Climate and Emission Changes on Stratospheric Aerosols and Ozone, Journal of the Atmospheric Sciences, 59, 414–440, https://doi.org/10.1175/1520-0469(2002)059<0414:IOFCAE>2.0.CO;2, place: Boston MA, USA Publisher: American Meteorological Society, 2002.

495   Pitari, G., Aquila, V., Kravitz, B., Robock, A., Watanabe, S., Cionni, I., Luca, N. D., Genova, G. D., Mancini, E., and Tilmes, S.: Stratospheric ozone response to sulfate geoengineering: Results from the Geoengineering Model Intercomparison Project (GeoMIP), Journal of Geophysical Research: Atmospheres, 119, 2629–2653, https://doi.org/10.1002/2013JD020566, 2014.

Richter, J. H., Tilmes, S., Mills, M. J., Tribbia, J. J., Kravitz, B., Macmartin, D. G., Vitt, F., and Lamarque, J. F.: Stratospheric dynamical response and ozone feedbacks in the presence of SO2 injections, Journal of Geophysical Research: Atmospheres, 122, 12,557–12,573,
500   https://doi.org/10.1002/2017JD026912, 2017.

Robock, A.: Volcanic eruptions and climate, Reviews of Geophysics, 38, 191–219, https://doi.org/10.1029/1998RG000054, 2000.

Roehl, C. M., Boglu, D., Brühl, C., and Moortgat, G. K.: Infrared band intensities and global warming potentials of CF4, C2F6, C3F8, C4F10, C5F12, and C6F14, Geophysical Research Letters, 22, 815–818, https://doi.org/https://doi.org/10.1029/95GL00488, 1995.

Sandoval-Soto, L., Stanimirov, M., von Hobe, M., Schmitt, V., Valdes, J., Wild, A., and Kesselmeier, J.: Global uptake of carbonyl sulfide
505   (COS) by terrestrial vegetation: Estimates corrected by deposition velocities normalized to the uptake of carbon dioxide (CO_2), Biogeosciences, 2, 125–132, https://doi.org/10.5194/bg-2-125-2005, 2005.

Smith, C. J., Kramer, R. J., Myhre, G., Alterskjær, K., Collins, W., Sima, A., Boucher, O., Dufresne, J.-L., Nabat, P., Michou, M., Yukimoto, S., Cole, J., Paynter, D., Shiogama, H., O'Connor, F. M., Robertson, E., Wiltshire, A., Andrews, T., Hannay, C., Miller, R., Nazarenko, L., Kirkev\aag, A., Olivié, D., Fiedler, S., Lewinschal, A., Mackallah, C., Dix, M., Pincus, R., and Forster, P. M.: Effective radiative forcing
510   and adjustments in CMIP6 models, Atmospheric Chemistry and Physics, 20, 9591–9618, https://doi.org/10.5194/acp-20-9591-2020, 2020.

Smith, W. and Wagner, G.: Stratospheric aerosol injection tactics and costs in the first 15 years of deployment, Environmental Research Letters, 13, 124 001, https://doi.org/10.1088/1748-9326/aae98d, 2018.

Steinbacher, M., Bingemer, H. G., and Schmidt, U.: Measurements of the exchange of carbonyl sulfide (OCS) and carbon disulfide (CS2) between soil and atmosphere in a spruce forest in central Germany, Atmospheric Environment, 38, 6043–6052,
515   https://doi.org/https://doi.org/10.1016/j.atmosenv.2004.06.022, 2004.

Tilmes, S., Müller, R., and Salawitch, R.: The Sensitivity of Polar Ozone Depletion to Proposed Geoengineering Schemes, Science, 320, 1201–1204, https://doi.org/10.1126/science.1153966, 2008.

Tilmes, S., Garcia, R. R., Kinnison, D. E., Gettelman, A., and Rasch, P. J.: Impact of geoengineered aerosols on the troposphere and stratosphere, Journal of Geophysical Research: Atmospheres, 114, https://doi.org/https://doi.org/10.1029/2008JD011420, 2009.

520   Tilmes, S., Mills, M. J., Niemeier, U., Schmidt, H., Robock, A., Kravitz, B., Lamarque, J.-F., Pitari, G., and English, J. M.: A new Geoengineering Model Intercomparison Project (GeoMIP) experiment designed for climate and chemistry models, Geoscientific Model Development, 8, 43–49, https://doi.org/10.5194/gmd-8-43-2015, 2015.

Tilmes, S., Richter, J. H., Kravitz, B., Macmartin, D. G., Mills, M. J., Simpson, I. R., Glanville, A. S., Fasullo, J. T., Phillips, A. S., Lamarque, J. F., Tribbia, J., Edwards, J., Mickelson, S., and Ghosh, S.: CESM1(WACCM) stratospheric aerosol geoengineering large ensemble
525   project, Bulletin of the American Meteorological Society, pp. 2361–2371, https://doi.org/10.1175/BAMS-D-17-0267.1, 2018a.

Tilmes, S., Richter, J. H., Mills, M. J., Kravitz, B., MacMartin, D. G., Garcia, R. R., Kinnison, D. E., Lamarque, J. F., Tribbia, J., and Vitt, F.: Effects of Different Stratospheric SO2 Injection Altitudes on Stratospheric Chemistry and Dynamics, Journal of Geophysical Research: Atmospheres, 123, 4654–4673, https://doi.org/10.1002/2017JD028146, 2018b.

Tilmes, S., Richter, J. H., MacMartin, D. G., Kravitz, B., Glanville, A., Visioni, D., , Kinnison, D., and Mueller, R.: Sensitivity of total
530   column ozone to stratospheric sulfur injection strategies, Geophysical Research Letters, n/a, n/a, inreview, 2021.

Trisos, C. H., Amatulli, G., Gurevitch, J., Robock, A., Xia, L., and Zambri, B.: Potentially dangerous consequences for biodiversity of solar geoengineering implementation and termination, Nature Ecology & Evolution, 2, 475–482, https://doi.org/10.1038/s41559-017-0431-0, 2018.

Ulshofer, V., Flock, O., Uher, G., and Andreae, M.: Photochemical production and air-sea exchange of carbonyl sulfide in the eastern
535   Mediterranean Sea, Marine Chemistry, 53, 25–39, 1996.

Van Diest, H. and Kesselmeier, J.: Soil atmosphere exchange of carbonyl sulfide (COS) regulated by diffusivity depending on water-filled pore space, Biogeosciences, 5, 475–483, https://doi.org/10.5194/bg-5-475-2008, 2008.

Vattioni, S., Weisenstein, D., Keith, D., Feinberg, A., Peter, T., and Stenke, A.: Exploring accumulation-mode H2SO4 versus SO2 strato-spheric sulfate geoengineering in a sectional aerosol-chemistry-climate model, Atmospheric Chemistry and Physics, 19, 4877–4897,
540   https://doi.org/10.5194/acp-19-4877-2019, 2019.

Visioni, D., Pitari, G., Aquila, V., Tilmes, S., Cionni, I., Di Genova, G., and Mancini, E.: Sulfate geoengineering impact on methane transport and lifetime: results from the Geoengineering Model Intercomparison Project (GeoMIP), Atmospheric Chemistry and Physics, 17, 11 209–11 226, https://doi.org/10.5194/acp-17-11209-2017, 2017a.

Visioni, D., Pitari, G., Aquila, V., Tilmes, S., Cionni, I., Di Genova, G., and Mancini, E.: Sulfate geoengineering impact on methane transport
545   and lifetime: results from the Geoengineering Model Intercomparison Project (GeoMIP), Atmospheric Chemistry and Physics, 17, 11 209–11 226, https://doi.org/10.5194/acp-17-11209-2017, 2017b.

Visioni, D., Pitari, G., Di Genova, G., Tilmes, S., and Cionni, I.: Upper tropospheric ice sensitivity to sulfate geoengineering, Atmospheric Chemistry and Physics, https://doi.org/10.5194/acp-18-14867-2018, 2018a.

Visioni, D., Pitari, G., Tuccella, P., and Curci, G.: Sulfur deposition changes under sulfate geoengineering conditions: Quasi-biennial oscil-
550   lation effects on the transport and lifetime of stratospheric aerosols, Atmospheric Chemistry and Physics, https://doi.org/10.5194/acp-18-2787-2018, 2018b.

Visioni, D., Pitari, G., Tuccella, P., and Curci, G.: Sulfur deposition changes under sulfate geoengineering conditions: quasi-biennial oscillation effects on the transport and lifetime of stratospheric aerosols, Atmospheric Chemistry and Physics, 18, 2787–2808, https://doi.org/10.5194/acp-18-2787-2018, 2018c.

555   Visioni, D., MacMartin, D. G., Kravitz, B., Tilmes, S., Mills, M. J., Richter, J. H., and Boudreau, M. P.: Seasonal Injection Strategies for Stratospheric Aerosol Geoengineering, Geophysical Research Letters, 46, 7790–7799, https://doi.org/10.1029/2019GL083680, 2019.

Visioni, D., MacMartin, D. G., Kravitz, B., Lee, W., Simpson, I. R., and Richter, J. H.: Reduced Poleward Transport Due to Stratospheric Heating Under Stratospheric Aerosols Geoengineering, Geophysical Research Letters, 47, e2020GL089 470, https://doi.org/https://doi.org/10.1029/2020GL089470, e2020GL089470 10.1029/2020GL089470, 2020.

560   Visioni, D., MacMartin, D. G., and Kravitz, B.: Is Turning Down the Sun a Good Proxy for Stratospheric Sulfate Geoengineering?, Journal of Geophysical Research: Atmospheres, 126, e2020JD033 952, https://doi.org/https://doi.org/10.1029/2020JD033952, e2020JD033952 2020JD033952, 2021.

Wang, L., Yang, Y., Shen, W., Kong, X., Li, P., Yu, J., and Rodrigues, A. E.: CO2 Capture from Flue Gas in an Existing Coal-Fired Power Plant by Two Successive Pilot-Scale VPSA Units, Industrial & Engineering Chemistry Research, 52, 7947–7955, 2013.

565 West, J. J. and Fiore, A. M.: Management of Tropospheric Ozone by Reducing Methane Emissions, Environmental Science & Technology, 39, 4685–4691, https://doi.org/10.1021/es048629f, pMID: 16053064, 2005.

Whelan, M. E., Hilton, T. W., Berry, J. A., Berkelhammer, M., Desai, A. R., and Campbell, J. E.: Carbonyl sulfide exchange in soils for better estimates of ecosystem carbon uptake, Atmospheric Chemistry and Physics, 16, 3711–3726, 2016.

Xia, L., Nowack, P. J., Tilmes, S., and Robock, A.: Impacts of stratospheric sulfate geoengineering on tropospheric ozone, Atmospheric

570 Chemistry and Physics, 17, 11 913–11 928, https://doi.org/10.5194/acp-17-11913-2017, 2017a.

Xia, L., Nowack, P. J., Tilmes, S., and Robock, A.: Impacts of stratospheric sulfate geoengineering on tropospheric ozone, Atmospheric Chemistry and Physics, 17, 11 913–11 928, https://doi.org/10.5194/acp-17-11913-2017, 2017b.